

Impact of Hole-Transport Layer and Interface Passivation on Halide Segregation in Mixed-Halide Perovskites

Vincent J.-Y. Lim, Alexander J. Knight, Robert D. J. Oliver, Henry J. Snaith, Michael B. Johnston, and Laura M. Herz*

Mixed-halide perovskites offer ideal bandgaps for tandem solar cells, but photoinduced halide segregation compromises photovoltaic device performance. This study explores the influence of a hole-transport layer, necessary for a full device, by monitoring halide segregation through in situ, concurrent X-ray diffraction and photoluminescence measurements to disentangle compositional and optoelectronic changes. This work demonstrates that top coating $\text{FA}_{0.83}\text{Cs}_{0.17}\text{Pb}(\text{Br}_{0.4}\text{I}_{0.6})_3$ perovskite films with a poly(triaryl)amine (PTAA) hole-extraction layer surprisingly leads to suppression of halide segregation because photogenerated charge carriers are rapidly trapped at interfacial defects that do not drive halide segregation. However, the generation of iodide-enriched regions near the perovskite/PTAA interface enhances hole back-transfer from the PTAA layer through improved energy level offsets, increasing radiative recombination losses. It is further found that while passivation with a piperidinium salt slows halide segregation in perovskite films, the addition of a PTAA top-coating accelerates such effects, elucidating the specific nature of trap types that are able to drive the halide segregation process. This work highlights the importance of selective passivation techniques for achieving efficient and stable wide-bandgap perovskite photovoltaic devices.

performance has been attributed to excellent optoelectronic properties including high absorbance,^[6] long charge-carrier lifetimes and diffusion lengths,^[7,8] as well as a high defect tolerance^[9,10] and good crystallinity.^[11,12] Another advantageous property of MHPs is the facile tuneability of their bandgap (between ≈ 1.2 and 2.3 eV),^[1,12–17] which can be achieved by tuning the perovskite chemical composition (ABX_3 , where A is a cation, B is a divalent metal, and X is a halide). Since the frontier orbitals of MHPs largely derive from the metal and halide contributions,^[18] substitutions on these sites are particularly effective for tuning the bandgap.^[14,17,19] Such bandgap engineering is essential for photovoltaic tandem cells, which require stacks of absorber materials with optimized bandgaps to deliver excellent power conversion efficiencies that substantially exceed those of single-junction devices.^[20–23]

The ideal light-facing, high-bandgap subcell in a perovskite-perovskite or perovskite-silicon tandem photovoltaic cell is often achieved by alloying bromide


and iodide on the halide site, yielding $\text{APb}(\text{Br}_x\text{I}_{1-x})_3$ compositions,^[21,22] where the A-cation site is usually occupied by methylammonium (MA^+), formamidinium (FA^+), cesium (Cs^+), or a mixture thereof. While alloying different halide species permits easy manipulation of the bandgap, it unfortunately also introduces a compositional instability problem under illumination, known as halide segregation or photoinduced phase segregation.^[16,24] During this process, halide ions migrate to segregate into regions of iodide-enriched and bromide-enriched composition when excited charge carriers are present, either through photoexcitation^[16,25,26] or current injection.^[27–29] Low energetic barriers toward halide ion movement in MHPs,^[30,31] especially along grain boundaries,^[32–34] promote such phase segregation. It is also observed that once the illumination or current injection source is removed, recovery of segregated mixed-halide perovskites back to their pristine mixed-phase state is observed as a result of entropic mixing.^[16,26,35] Iodide-rich domains formed during halide segregation possess a lower bandgap compared to that of the original mixed-phase composition.^[16,17,19,36,37] Excited charge carriers generated in the majority mixed-halide material therefore funnel into newly-created iodide-rich minority regions to minimize their energy,

1. Introduction

Metal halide perovskites (MHPs) have been subjected to intense research over the past decade owing to their emergence as photoactive layers in efficient photovoltaic devices.^[1–5] Their

V. J.-Y. Lim, A. J. Knight, R. D. J. Oliver, H. J. Snaith, M. B. Johnston, L. M. Herz
Department of Physics
University of Oxford
Clarendon Laboratory, Parks Road, Oxford OX1 3PU, UK
E-mail: laura.herz@physics.ox.ac.uk

L. M. Herz
Institute for Advanced Study
Technical University of Munich
Lichtenbergstrasse 2a, D-85748 Garching, Germany

 The ORCID identification number(s) for the author(s) of this article can be found under <https://doi.org/10.1002/adfm.202204825>.

© 2022 The Authors. Advanced Functional Materials published by Wiley-VCH GmbH. This is an open access article under the terms of the Creative Commons Attribution License, which permits use, distribution and reproduction in any medium, provided the original work is properly cited.

DOI: 10.1002/adfm.202204825

resulting in red-shifted photoluminescence spectra. Halide segregation compromises the performance of MHP solar cells through accelerated radiative recombination within iodide-rich regions where charge carriers concentrate, lowering the open-circuit voltage^[38–41] and current extraction efficiency.^[24,29,42]

While halide segregation has clear impact on MHP tandem device development, most investigations to date have investigated the phenomenon through relatively straightforward observation of the evolution of photoluminescence spectra of standalone MHP films under illumination.^[16,24] However, this approach ignores the influence of charge-transport layers (CTLs) interfacing MHP layers, which are fundamental to the architecture of real-world MHP photovoltaic devices.^[43,44] Knowledge of how charge-transport layers affect halide segregation is particularly crucial because it is well known that MHP/CTL interfaces exhibit high trap densities,^[45–47] and also that electronic trap states can be important instigators of halide segregation.^[24,42,48–50] We note that while there are previous studies of halide segregation in device stacks,^[28,29,39] only a few studies have methodologically investigated the impact of charge-transport layers on halide segregation,^[51,52] and an understanding of how trap states affect such segregation is still lacking. In particular, it has been proposed that only a subset of electronic traps appear to be associated with halide segregation,^[42,53] therefore a distinction is beneficial between the impact of traps present in the MHP bulk and those introduced at the MHP/CTL interface. In addition, the prominent use of photoluminescence techniques to reflect the extent to which halide segregation has occurred has been shown to be misleading at times,^[54] because the spectra collected not only represent the fraction of the material present in the phase-segregated state, but also the extent to which charge-carriers diffuse to iodide-enriched, low-energy domains. In the presence of a CTL competing with iodide-rich domains for charge-carrier collection, any changes in PL spectra over time may therefore be potentially unable to capture accurately the true extent to which halide segregation has occurred.

In this study, we have investigated the effects of a hole-transport layer (HTL) and trap passivation on halide segregation in the lead mixed-halide perovskite $\text{FA}_{0.83}\text{Cs}_{0.17}\text{Pb}(\text{Br}_{0.4}\text{I}_{0.6})_3$ whose bandgap of 1.79 eV is optimised for use in all-perovskite tandem photovoltaic devices.^[55] Compared to the mixed wide-bandgap phase, the iodide-rich regions formed during halide segregation are known to have a higher valence band edge but relatively unchanged conduction band edge.^[56,57] We thus expect halide segregation to affect charge-carrier dynamics mostly in the presence of a HTL, and therefore focus on such effects here. Through a combined approach of in situ, simultaneous X-ray diffraction (XRD) and photoluminescence (PL) spectroscopy, we are able to disentangle the structural effects of halide segregation from its impact on optoelectronic properties, showing that in the presence of hole-transport layers, an assessment of halide segregation from photoluminescence measurements alone can be highly misleading. Our analysis reveals that the presence of a typical poly(triaryl amine) (PTAA) hole-transport layer surprisingly lowers the extent to which halide segregation occurs. This effect primarily results from the removal of holes from the bulk of the MHP, as a result of them being trapped at the MHP/PTAA interface and holes drifting into the

PTAA. We show that the highly abundant interfacial trap states at the MHP/PTAA interface do not drive halide segregation, and are efficiently passivated by a piperidinium salt. Interestingly, the removal of trap states at the MHP/PTAA interface leads to more halide segregation being observed, as determined from XRD measurements. This is because charge carriers are no longer populating these interfacial states, and instead accumulate in bulk trap states that do drive the segregation process. These findings thus demonstrate the effect of an HTL on the halide segregation process and underline the need for passivation strategies tuned to eliminate the specific type of trap states that drive halide segregation.

2. Results and Discussion

$\text{FA}_{0.83}\text{Cs}_{0.17}\text{Pb}(\text{Br}_{0.4}\text{I}_{0.6})_3$ is relevant to all-perovskite and perovskite/silicon tandem cell applications as the top (wide bandgap) subcell,^[20–22] owing to its superior stability, compared to MA-based MHPs,^[37,58,59] and its ideal bandgap.^[37] Samples were fabricated on z-cut quartz substrates, as detailed in Section 4, with one set of MHP films being over-coated with a poly(triaryl amine) (PTAA) hole-transport layer,^[57] and another with an inert layer of poly(methyl methacrylate) (PMMA) to act as a control system. Ambient air is known to interact with MHPs and affect their PL transients^[60–62] and halide segregation dynamics,^[48,63] therefore the PMMA coating was chosen to eliminate such interactions with ambient gas by providing encapsulation in the absence of electronic interactions with the MHP.^[54] Each set of MHP samples were further fabricated either with or without a piperidinium ionic additive (1-butyl-1-methylpiperidinium tetrafluoroborate ($[\text{BMP}]^+[\text{BF}_4]^-$)) that has recently been reported to effectively passivate traps occurring near the boundary between the perovskite photoactive layer and the hole-transport layer.^[64,65] The addition of the piperidinium salt to the MHP layer enabled us to investigate halide segregation in real-world conditions, for which effective passivation strategies are likely to have been deployed. Moreover, the piperidinium additive enabled us to distinguish the electronic effects of adding a PTAA layer from those arising solely from the introduction of interfacial trap states at the MHP/PTAA boundary. Absorption spectra measured for these four thin-film combinations (either with PTAA or PMMA coating, with or without piperidinium salt), as well as two further MHP films without any coating, show that neither the coating nor the addition of piperidinium affected the absorption spectra of the $\text{FA}_{0.83}\text{Cs}_{0.17}\text{Pb}(\text{Br}_{0.4}\text{I}_{0.6})_3$ perovskite in the wavelength region of interest, as presented in Figure S1 (Supporting Information), and this is in agreement with the observations of Oliver et al., who showed such piperidinium additive had negligible effect on the fundamental electronic structure of the MHP.^[65]

To explore halide segregation in $\text{FA}_{0.83}\text{Cs}_{0.17}\text{Pb}(\text{Br}_{0.4}\text{I}_{0.6})_3$ in the presence of a HTL, we employed an in situ, concurrent XRD and PL measurement approach described previously elsewhere^[54] and in Section 4. XRD and PL have commonly been used as two separate techniques to characterize the extent to which halide segregation has occurred in a mixed-halide MHP.^[16,29,50,66–68] However, their in situ combination presents distinct advantages because the two techniques probe different

aspects of the material. While XRD probes structural properties evenly across the bulk material, PL spectra reflect the optoelectronic properties of the MHP, and specifically the material regions where radiative recombination of charge carriers is prevalent. For the specific case of monitoring halide segregation, XRD will accurately reflect the extent to which the materials have structurally segregated in the bulk, while PL will in addition be highly influenced by charge-carrier funnelling into iodide-rich regions.^[41] The combination of these two measurement techniques is particularly important for this study, since the presence of the PTAA layer will lead to charge extraction from the MHP by equilibrating the quasi-Fermi levels.^[69] The optoelectronic and structural properties reflected in the PL and XRD may therefore be affected in different ways depending on the presence of PTAA, as well as the piperidinium additive.

We begin our analysis by contrasting halide segregation during illumination for $\text{FA}_{0.83}\text{Cs}_{0.17}\text{Pb}(\text{Br}_{0.4}\text{I}_{0.6})_3$ thin films top-coated with either a PTAA hole-extraction layer or an inert PMMA layer. We note that MHP thin films in absence of any coating layers were also examined (see Figure S3, Supporting Information); however, these films exhibit qualitative behavior similar to that of the PMMA-coated MHP films. Those without any coating layers do exhibit some fluctuations in the PL spectra, which have previously been shown to be caused by interactions with ambient air.^[48] This observation implies that the

PMMA and PTAA top layers are sufficiently effective encapsulants to prevent such fluctuations arising from the interactions between ambient air and the MHP layer.^[48] **Figure 1** contrasts the PL spectra (top) and (220) X-ray diffraction peak (bottom) of $\text{FA}_{0.83}\text{Cs}_{0.17}\text{Pb}(\text{Br}_{0.4}\text{I}_{0.6})_3$ films without piperidinium additive, coated with either a PMMA (left) or PTAA (right) top layer, recorded concurrently in situ over ≈ 5 h of illumination with a continuous wave, 470 nm wavelength laser at 190 mW cm^{-2} intensity, ≈ 3.5 sun equivalent photon flux at this bandgap. The XRD peak selected for investigation was the (220) peak, comparable to earlier measurements.^[54] This choice aimed to maximise the XRD signal, and a second-order peak was selected (as opposed to the first order (110) peak) to improve the angular resolution.

The first striking observation to be made from these measurements is that the introduction of a PTAA hole-extraction layer leads to significantly enhanced radiative recombination of charge carriers from iodide-rich domains formed by halide segregation in $\text{FA}_{0.83}\text{Cs}_{0.17}\text{Pb}(\text{Br}_{0.4}\text{I}_{0.6})_3$. Figure 1a,b displays the PL spectra of PMMA- and PTAA-coated MHP, respectively, scaled by equating the peak intensity values of their respective initial spectra at the beginning of illumination (time = 0) to unity. For both cases, the initial photoluminescence spectra reflect the entropically mixed state (peak at 720 nm), but under laser illumination, a secondary PL peak at a higher wavelength (at 780 nm)

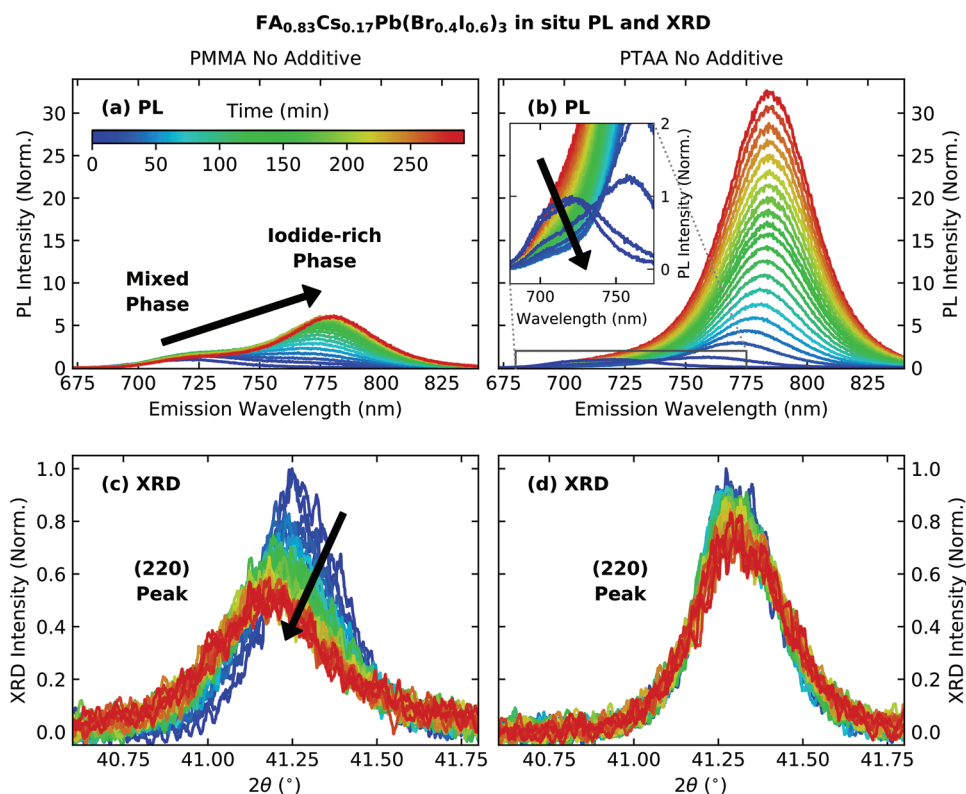


Figure 1. In situ, simultaneously recorded PL spectra and XRD patterns, recorded in ambient air for $\text{FA}_{0.83}\text{Cs}_{0.17}\text{Pb}(\text{Br}_{0.4}\text{I}_{0.6})_3$ thin films coated with either PMMA or PTAA under 470 nm continuous wave illumination with 190 mW cm^{-2} intensity for ≈ 5 h. a) PL spectra, normalized to the maximum value of the spectrum at time = 0, for an $\text{FA}_{0.83}\text{Cs}_{0.17}\text{Pb}(\text{Br}_{0.4}\text{I}_{0.6})_3$ thin film coated with PMMA. b) PL spectra, normalized to the spectrum at time = 0, for an $\text{FA}_{0.83}\text{Cs}_{0.17}\text{Pb}(\text{Br}_{0.4}\text{I}_{0.6})_3$ thin film coated with PTAA. (inset) An enlarged view of the PL spectra with finer time steps between consecutive spectra, with those for earliest illumination times shown in blue. c) Evolution of the (220) X-ray diffraction peak of an $\text{FA}_{0.83}\text{Cs}_{0.17}\text{Pb}(\text{Br}_{0.4}\text{I}_{0.6})_3$ thin film coated with PMMA, recorded in situ and simultaneously with PL measurements shown in (a). d) Evolution of the (220) XRD peak of an $\text{FA}_{0.83}\text{Cs}_{0.17}\text{Pb}(\text{Br}_{0.4}\text{I}_{0.6})_3$ thin film coated with PTAA, recorded in situ and simultaneously with (b). $\text{Cu-K}_{\alpha 1}$ line was used as the incident radiation for (c) and (d).

grows with time. This low-energy PL peak corresponds to photoemission from iodide-rich regions with a lower bandgap, reflecting progressing halide segregation.^[16,24,66] However, the two top layers clearly induce a different extent of low-energy PL enhancement: while the PTAA-coated MHP exhibits much more substantial growth in low-energy (high-wavelength) PL intensity with respect to the initial mixed-phase PL, by a factor of ≈ 32 , the PMMA-coated MHP only exhibits an approximately sixfold increase. Another way in which the qualitative behavior differs between the two scenarios is that the initial mixed-phase emission peak is always present to some extent for the PMMA-coated MHP (Figure 1a, blue line, consistent with previous reports^[54]), whereas this peak quickly and entirely disappears for the PTAA-coated MHP (see inset in Figure 1b). We stress that at this point, these results solely reveal that the addition of a PTAA top layer results in substantially increased radiative charge-carrier recombination from iodide-rich domains in the phase-segregated MHP (compared to the case of adding an inert PMMA top-layer).

Such enhanced emission from phase-segregated domains in PTAA-coated $\text{FA}_{0.83}\text{Cs}_{0.17}\text{Pb}(\text{Br}_{0.4}\text{I}_{0.6})_3$ may at a cursory glance suggest that the addition of a HTL layer leads to increased phase segregation in the MHP. However, our analysis of the evolution of the MHP's XRD peak shows this conclusion to be erroneous, with the illuminated bulk MHP film actually showing a far lower extent of structural re-organisation for PTAA-coating (Figure 1d) than for PMMA-coating (Figure 1c). We note that XRD is a far more accurate measure of the extent to which halide segregation has occurred compared to PL measurements, owing to its sensitivity to structural changes occurring across the full material volume. Because bromide and iodide ions have different radii and bond lengths, the lattice parameters of the MHP shift with the local average composition of the halide site.^[16,17,36,37,70] Rearrangement of these halide ions will therefore affect the local lattice parameter, which will alter the overall distribution of lattice parameters reflected in the XRD pattern. After halide segregation, the XRD patterns will reflect the changes in the lattice parameters from the presence of additional iodide- and bromide-enriched material, as well as remnants of the original well-mixed phase.^[54] We note that other factors, including lattice strain, atomic form factor, crystallinity, and material degradation may also potentially affect the XRD response (further discussed in Section S4, Supporting Information). However, we find, through angle-integration across the (220) XRD peak (Figure S5, Supporting Information), that the XRD intensity is constant with illumination time, indicating that the overall perovskite structure is maintained. In addition, full XRD patterns recorded after halide segregation (Figure S4, Supporting Information) reveal an absence of chemical degradation e.g. to crystalline PbI_2 , therefore halide segregation is the dominant process occurring under illumination. Knight et al. investigated degradation of related samples under similar conditions and observed negligible degradation.^[54]

The evolution of the $\text{FA}_{0.83}\text{Cs}_{0.17}\text{Pb}(\text{Br}_{0.4}\text{I}_{0.6})_3$ XRD peaks, shown in Figure 1c,d, clearly indicates that the PMMA-coated MHP exhibits significantly stronger halide segregation compared to the PTAA-coated MHP. The (220) XRD peak of the PMMA-coated MHP indicates an enhancement of diffraction amplitudes at angles below the peak of the original mixed-

halide phase, caused by a growth in iodide-rich material, and a rise in high-angle signal resulting from bromide-enriched phases, as can be more clearly seen in Figure S6 (Supporting Information).^[54] In contrast, the XRD peak of the PTAA-coated MHP only exhibits relatively minor changes with time under illumination. Taken together, the combined PL and XRD measurements therefore demonstrate that coating the MHP with a PTAA layer results in significant suppression of bulk halide rearrangement. However, in spite of this suppression, a larger fraction of charge carriers recombines in iodide-rich domains, leading to an enhancement of low-energy PL that is far greater for PTAA coating than for the case of PMMA coating. These results therefore demonstrate that the significantly stronger enhancement of the PL from iodide-rich domains for the PTAA-coated MHP arises from the altered charge-carrier dynamics, rather than enhanced halide segregation. Our combined, in situ XRD/PL technique therefore also demonstrates that analysis of halide segregation from PL spectral evolution alone can be highly misleading, in particular in the presence of charge-extraction layers.

To understand the differences in halide segregation and PL emission between PTAA- and PMMA-coated $\text{FA}_{0.83}\text{Cs}_{0.17}\text{Pb}(\text{Br}_{0.4}\text{I}_{0.6})_3$, we consider the optoelectronic changes occurring upon halide segregation at the MHP/PTAA interface. Figure 2 schematically depicts the simplified energy level scheme near the MHP/PTAA interface, based on literature values.^[56,57,69] The valence band edge (or highest occupied molecular orbital) of PTAA is higher in energy compared to the valence band edge of $\text{FA}_{0.83}\text{Cs}_{0.17}\text{Pb}(\text{Br}_{0.4}\text{I}_{0.6})_3$, so that before halide segregation has occurred (Figure 2a), holes in the MHP layer diffuse toward and are captured by the PTAA layer. The energy gap between the valence bands of the mixed-phase MHP and the PTAA layer presents a significant energetic barrier towards the back-transfer of holes from PTAA back into the MHP, as desirable in a photovoltaic device. Before halide segregation commences, charge carriers are therefore likely to recombine non-radiatively, e.g., via interfacial trap states, rather than radiatively in the MHP following hole re-transfer to the MHP. The accumulation of holes within the PTAA layer is likely to influence the region in which halide segregation nucleates under prolonged illumination; hole accumulation will lead to a net positive charge within the PTAA layer, which will attract electrons in the MHP layer coulombically towards the MHP/PTAA interface. The high charge-carrier density near the interface means that any limited amount of halide segregation present in this configuration with PTAA will be more concentrated near the interface, rather than spread throughout the bulk. Accordingly, the charge-carrier density remaining in the bulk of the MHP layer will be relatively depleted, lowering the propensity for halide segregation to occur far from the interface. These considerations also explain our observation (from XRD) of the presence of the PTAA layer reducing halide segregation because charge carriers driving such segregation are effectively removed from the bulk, e.g., through hole collection into PTAA or fast charge trapping at interface states.

The prevalence of halide segregation near the MHP/PTAA interface further explains the observation of enhanced photoluminescence from iodide-rich regions following illumination (Figure 1b). As schematically illustrated in Figure 2b, the

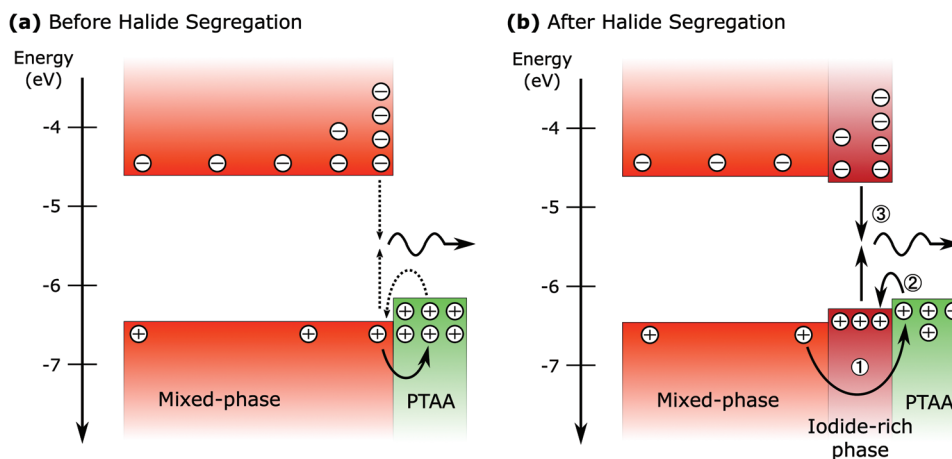


Figure 2. Schematic diagram illustrating the dynamics of charge carriers in a MHP/PTAA partial device before and after halide segregation. a) Before halide segregation has occurred, photogenerated holes in the MHP diffuse into the PTAA layer, but only a small minority is able to transfer back into the MHP owing to the large energy offset at the interface. Such minority back-transfer allows for relatively faint radiative recombination with electrons, yielding photoluminescence spectra representative of the mixed phase. The accumulation of holes in the PTAA layer coulombically attracts electrons towards the MHP/PTAA interface. b) After halide segregation has occurred, photoexcited holes diffuse into the PTAA layer (1), and a more significant proportion of these holes later back-transfer preferentially into iodide-rich regions within the MHP layer, owing to the smaller energy gap compared with the mixed phase (2). These holes subsequently recombine radiatively with electrons, yielding red-shifted photoluminescence characteristic of iodide-rich regions (3). Energy levels shown are relative to the vacuum level, and were extrapolated based on previous reports.^[56,57] Bromide-rich regions formed after halide segregation are not indicated, since their wider bandgap and unfavourable energy alignment mean that charge carriers generally cannot be injected into these from mixed-phase or iodide-rich regions.

introduction of an iodide-rich phase near the interface alters the band alignment in this region toward more favorable back-transfer of holes into the MHP, where they may recombine radiatively. The newly introduced iodide-rich regions are associated with an upshift in valence band maximum compared to that of the mixed phase,^[56,71] resulting in a smaller energy difference with respect to the PTAA band edge. This altered band alignment under illumination facilitates the back-transfer of holes from PTAA to iodide-rich regions near the interface (compared to a back-transfer into the original mixed-phase regions) leading to substantial radiative charge-carrier recombination in the iodide-rich MHP regions near the interface. In order to verify the better energy offset for iodide-rich regions with PTAA, we performed PL quantum yield (PLQY) measurements for an iodide-rich MHP of the composition $\text{FA}_{0.83}\text{Cs}_{0.17}\text{Pb}(\text{Br}_{0.1}\text{I}_{0.9})_3$, which is representative of that expected for iodide-rich regions occurring in $\text{FA}_{0.83}\text{Cs}_{0.17}\text{Pb}(\text{Br}_{0.4}\text{I}_{0.6})_3$ after halide segregation from the PL emission wavelength, with and without a PTAA top-coating layer. The relative PLQY quenching observed upon the introduction of a PTAA top-coating layer was lower for the iodide-rich MHP, compared to the wide-bandgap MHP (Table S1, Supporting Information). Such change in PLQY for the iodide-rich MHP as compared to the $\text{FA}_{0.83}\text{Cs}_{0.17}\text{Pb}(\text{Br}_{0.4}\text{I}_{0.6})_3$ MHP further corroborates that the PL enhancement is the direct result of improved band alignment for hole re-transfer and/or a reduction in traps upon iodide enrichment; this is in agreement with Oliver et al. who demonstrated a significant deviation between the quasi-fermi level splitting and open-circuit voltage for wide-bandgap MHP devices,^[65] and Stolterfoht et al. showing a smaller such offset for a low-bandgap (iodide-rich) MHP device.^[72]

The dynamic processes occurring in PTAA-coated $\text{FA}_{0.83}\text{Cs}_{0.17}\text{Pb}(\text{Br}_{0.4}\text{I}_{0.6})_3$ after halide segregation can therefore

be summarized as follows. Photogenerated holes diffuse into the PTAA layer (step 1 in Figure 2b), after which holes will preferentially funnel back into the iodide-rich regions induced by halide segregation near the interface (Figure 2b step 2). We note that bromide-rich regions will also form to conserve overall halide content, but charge carriers cannot enter these regions from mixed-phase or iodide-rich regions as they exhibit wider bandgap and unfavorable energy alignment. These bromide-rich regions will therefore have minimal optoelectronic effects, and are neglected accordingly in Figure 2b. A fraction of charge carriers recombines radiatively in these iodide-rich regions exhibiting lower bandgap (Figure 2b step 3), inducing intense red-shifted photoluminescence. These back-transfer effects also explain why no emission is observed from the original mixed-phase MHP: holes may diffuse rapidly from this phase into PTAA from which they will only transfer back effectively into iodide-rich regions.^[71] In contrast, the PMMA-coated MHP still features remnant emission from the mixed phase, even after substantial halide segregation has occurred (Figure 1a), since holes are neither drifted out, nor selectively reinjected into segregated phases, but rather diffuse into iodide-rich domains throughout the whole MHP layer. We therefore conclude that the significant enhancement of PL emission from iodide-rich domains in the presence of the hole-extraction layer is solely the result of charge-carrier dynamics occurring at and across the interface. The selective back-transfer of holes from PTAA to the MHP also explains the dramatic overall increase in PL intensity: high concentration of charge carriers in small iodide-enriched regions near the interface leads to particularly rapid radiative electron-hole bimolecular recombination, resulting in higher overall photoluminescence intensity.^[41,73,74]

We continue our investigation by exploring the reasons why halide segregation scarcely occurs when the MHP is top coated

with PTAA. Given that halide segregation is triggered by the presence of excited charge carriers,^[24,29,42] their rapid removal soon after photoexcitation could effectively limit halide segregation. The presence of a PTAA hole-transport layer may lead to holes either drifting from the MHP into the PTAA, or being trapped at defect states introduced at the interface, neither of which would occur in the presence of the inert PMMA layer. The interface between MHPs and typical charge-transport layers is known to possess an especially high density of trap states in general,^[45,46,69] and this has been shown to be also true for the MHP/PTAA interface for wide-bandgap MHPs.^[65] We further note that while some types of traps have been shown to aid halide segregation, others may not, but simply act to localize charge carriers.^[42] In order to understand why the addition of PTAA reduces halide segregation, we therefore need to distinguish the effects of hole extraction into PTAA from those of charge-carrier trapping at the MHP/PTAA interface. For this purpose, we employ a recently reported piperidinium additive that has been shown to be particularly effective in passivating trap states at MHP/CTL interfaces.^[64,65]

As a first step, we ascertained the extent to which the piperidinium ionic additive reduces charge-carrier trap state densities. For this purpose, we recorded time-resolved photoluminescence transients for $\text{FA}_{0.83}\text{Cs}_{0.17}\text{Pb}(\text{Br}_{0.4}\text{I}_{0.6})_3$ thin films before halide segregation had occurred, for the four combinations of the MHP having been coated with PTAA or PMMA layers, and with and without piperidinium ionic additive having been added. Further transients were also measured after halide segregation had occurred, as shown Figure S9 (Supporting Information). As shown in Figure 3, the piperidinium additive increases the lifetimes of the PL transients, implying an effective reduction in trap state density. The transients also confirm the high density of trap states introduced by the MHP/PTAA interface, given that the PTAA-coated MHPs

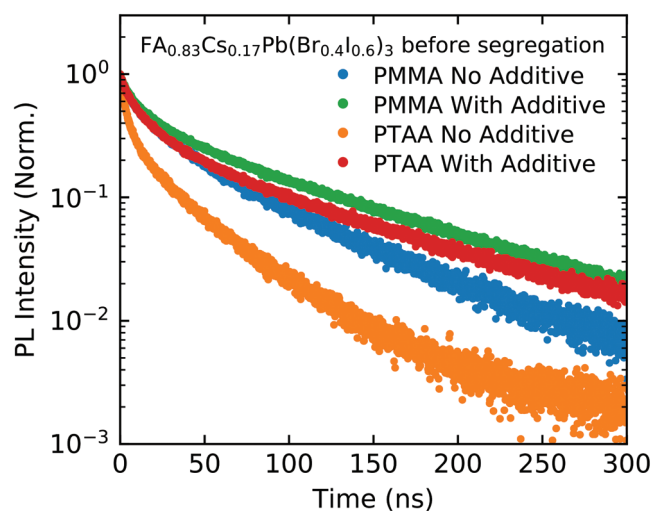


Figure 3. PL decay transients for $\text{FA}_{0.83}\text{Cs}_{0.17}\text{Pb}(\text{Br}_{0.4}\text{I}_{0.6})_3$ thin films coated with either PMMA or PTAA, with and without piperidinium salt having been added to the perovskite during processing. Films were excited with a pulsed laser (1 MHz repetition rate) at 470 nm with fluence of 15 nJ cm^{-2} and PL was detected at the wavelength of 700 nm corresponding to emission from the high-energy mixed phase of the perovskite, before any phase segregation had occurred under illumination.

exhibit significantly shorter charge-carrier lifetimes than the those coated with inert PMMA coating, in particular in the absence of piperidinium additive (see Section S6.1, Supporting Information, for extracted lifetimes). Meanwhile, the long charge-carrier lifetimes for the PMMA-coated MHPs further corroborate that the interface between inert PMMA and MHP layers is relatively benign. Trap state passivation upon the addition of piperidinium salt is evidently highly effective, with passivated films showing strikingly similar PL transients, regardless of the top-layer coating. It should also be noted that most likely, the piperidinium additive not only passivates interfacial trap states, but also bulk trap states to an extent, given the observed rise in charge-carrier lifetimes for the PMMA-coated MHPs upon the addition of piperidinium salt.

We find that once interfacial trap states have been removed through piperidinium ionic additive, both PMMA and PTAA-coated $\text{FA}_{0.83}\text{Cs}_{0.17}\text{Pb}(\text{Br}_{0.4}\text{I}_{0.6})_3$ films undergo halide segregation to an almost identical extent. Figure 4a,b shows that following $\approx 5 \text{ h}$ of illumination with 190 mW cm^{-2} intensity, the observed changes in the XRD patterns of the passivated MHP are very similar for both PMMA and PTAA coatings. Therefore, the suppression of halide segregation in PTAA-coated, unpassivated MHPs is simply caused by the unintentional introduction of a large density of interfacial traps, rather than hole collection into PTAA. As discussed in more detail in Section S4.2 (Supporting Information), the minor changes occurring in the XRD pattern under illumination for the unpassivated, PTAA-coated MHP film are also qualitatively different from those occurring in the rest of the MHPs, (the XRD peak angle does not change with illumination time) which we attribute to halide segregation occurring predominantly at the MHP/PTAA interface. Thus for PTAA top coating, the extent of halide segregation is almost fully governed by the density of trap states at the MHP/PTAA interface.

We note that for PMMA coating, which does not introduce significant interfacial trap states, the introduction of the piperidinium salt to the MHP has a very different effect. Figure 4c exhibits the XRD amplitude evolution during illumination for the four combinations of MHP films with either PMMA or PTAA coating, with or without piperidinium additive. We find that the rate of halide segregation in MHPs with the two different coatings are affected in opposite ways by piperidinium addition: while it accelerates halide segregation for the PTAA-coated MHPs, it slows down segregation for the PMMA-coated MHPs. We propose that such differences in the effect of the piperidinium additive on halide segregation stem from the different types of trap states present at the interface and in the bulk MHP. As discussed in more detail below, some trap states induce halide segregation, while others do not. The MHP/PTAA interface clearly presents a large number of trap states, but our results suggest that these do not drive halide segregation throughout significant volume of the MHP. Therefore, the presence of such interfacial trap states simply causes charge carriers to be trapped near the interface, as a result of which these carriers are unable to diffuse through the MHP bulk where they would otherwise have encountered traps that drive halide segregation. Rapid trapping of these charge carriers at the MHP/PTAA interface therefore suppresses halide segregation. For the case of PMMA-coated MHP films, traps exist

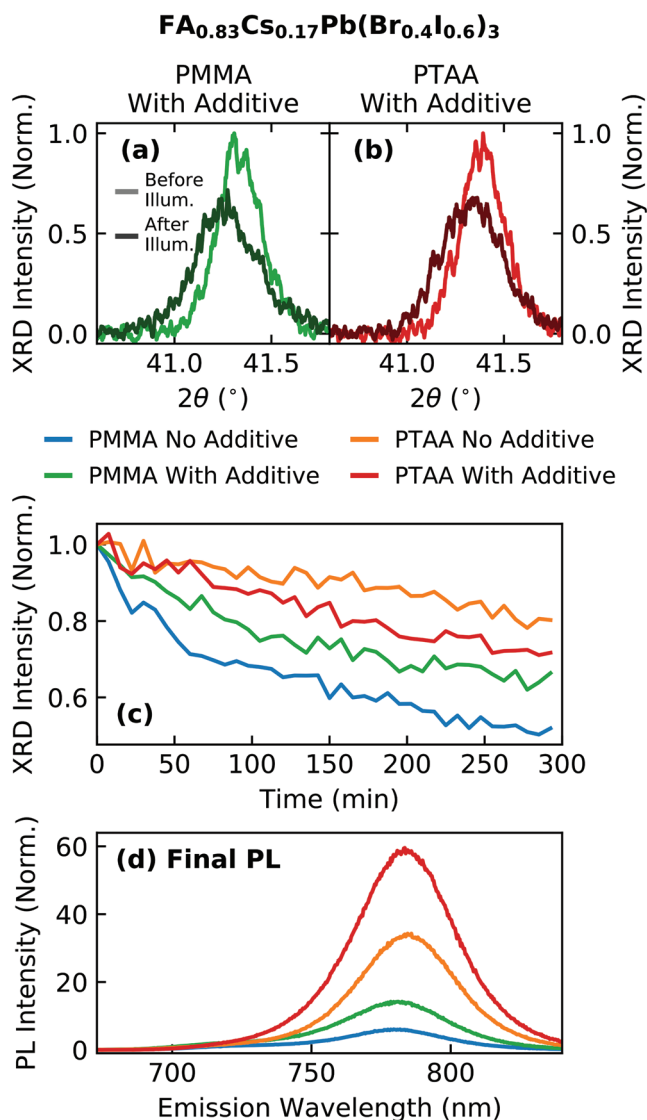


Figure 4. Second-order (220) XRD peak of FA_{0.83}CS_{0.17}Pb(Br_{0.4}I_{0.6})₃ films with piperidinium ionic additive, coated with either a) PMMA or b) PTAA, shown before and after illumination with a 470 nm laser at 190 mW cm⁻² intensity for ≈5 h. c) Evolution of the (220) XRD peak amplitude under the same illumination conditions for FA_{0.83}CS_{0.17}Pb(Br_{0.4}I_{0.6})₃ thin films with or without the addition of piperidinium salt, and with either PMMA and PTAA top coatings. d) Final PL spectra recorded in situ at the end of the ≈5 h illumination period, each normalized to the respective maximum value of the corresponding initial spectrum recorded when illumination had commenced. The raw data of the two films with piperidinium ionic additive can be found in Figure S2 (Supporting Information).

mostly in the bulk volume of the MHP and appear to be capable of driving halide segregation. The addition of piperidinium salt then passivates these bulk trap states to an extent, slowing down halide segregation, consistent with previous reports on the effects of trap passivation on halide segregation.^[24,49,50,52,75] In contrast, piperidinium passivation for the PTAA-coated film removes trap states at the interface, allowing bulk trap states to be populated and accelerate halide segregation. Thus, the overall extent of halide segregation is governed by a complex interplay of competition for charge carriers between interfacial

traps that do not induce halide segregation and bulk traps that are effective drivers of halide segregation. As a result, for PTAA-coated MHP, piperidinium mostly passivates interfacial trap states, accelerating halide segregation, while for PMMA-coated MHPs piperidinium additive passivates bulk traps, impeding halide segregation. We note that such trap passivation effects are clearly evident through an increase of the PL intensity upon the addition of piperidinium salt for both PMMA and PTAA-coated MHPs, shown in Figure 4d, and the increase in the charge carrier lifetimes discussed earlier (Figure 3).

We note that our conclusions are consistent with previous reports stipulating that only specific types of trap states are responsible for inducing halide segregation, while others are not.^[42,53] Such differences may, for example, be caused by local electric fields generated by captured charge carriers in trap states driving halide segregation.^[42,48,49,52,76,77] In this case, only initially charge-neutral defects might be responsible for halide segregation, as these will generate local charges once traps are filled. In addition, halide chemistry and oxidation has been postulated to be central to the halide segregation process.^[53] Overall, it is therefore evident that the nature of trap states is as central to their propensity to drive halide segregation as their density.

With regards to the specific effect of the piperidinium additive, we have employed as a passivation agent here, we note that Lin et al. demonstrated that it improved device stability by inhibition of lead oxidation, and proposed this was ultimately caused by either a reduction of iodide vacancy-interstitial pair Frenkel defects, or by reducing their diffusivity.^[64] This is in line with previous reports showing the abundance and stability of halide defects in MHPs.^[9,78–82] We therefore propose that the MHP/PTAA interface possesses a high density of charged halide interstitials and vacancies, the latter of which is filled with electrons upon steady-state photoexcitation, owing to the high density of electrons in the MHP layer at the interface (Figure 2b). Such halide vacancies, which also act as electronic trap states, become neutrally charged making them less effective at promoting halide segregation via electric fields. Additionally, the charge-neutral vacancies are less likely to be filled by halide ions, meaning that the interface then effectively becomes a halide-excess environment given the abundance of halide interstitials, in which halide segregation is impeded, as observed before,^[24,25,50,75,83,84] because the lack of available halide vacancies lowers the halide ion mobility. Upon the addition of the piperidinium salt, these halide defects become efficiently passivated. We note that while there are numerous reports demonstrating halide defects promoting halide segregation,^[25,84–86] we are not contradicting these, but rather proposing that the high concentration of electrons at the MHP/PTAA boundary could limit the effectiveness of halide ion migration through vacancies, and that the electronic nature of halide defect trap states does not contribute significantly to halide segregation, because of their neutral charge upon charge-carrier capture. In order for halide segregation to occur, the trap states that create an electric field are required, as well as halide defects to provide low-energy halide ion migration pathways.

We would like to comment that an enhancement of PL upon the addition of any generic HTL is expected for different MHP compositions, since the mechanism of such enhancement

relies on the favourable energy alignment between iodide-rich regions and HTL. However, we expect different HTL and passivation agents will affect the halide segregation behavior differently, depending on the fundamental nature of the trap states present at the MHP/HTL interface. Given the device-relevant FACs MHPs also exhibit a range of trap densities and difference in overall stability against halide segregation across the bromide-iodide ratio, we expect some variations as halide content is changed.^[12] The stability of a mixed-halide perovskite in the presence of an HTM against halide segregation therefore depends critically on the nature of the trap states present in the bulk and at the interfaces, and the chemical and physical mechanisms of passivation techniques deployed.

3. Conclusion

In conclusion, we have investigated the effects of hole-transport layers and trap passivation agents on halide segregation in a lead mixed-halide perovskite with bandgap optimized for use in tandem all-perovskite photovoltaic devices ($\text{FA}_{0.83}\text{Cs}_{0.17}\text{Pb}(\text{Br}_{0.4}\text{I}_{0.6})_3$). While observation of changes in PL spectra under illumination is most commonly used to assess the extent to which halide segregation occurs, we find here that such assessment can be highly misleading, in particular in the presence of hole-transport layers. We show that our combined approach—concurrently assessing the structural changes associated with halide segregation through XRD, and the optoelectronic changes with PL spectroscopy—is able to provide an accurate understanding of these processes. The presence of a hole-transport layer such as PTAA slows down halide segregation, compared to the case of inert PMMA (or absent) coating. This effect primarily results from the removal of charge carriers from the bulk of the perovskite by their capture into interfacial trap states at the MHP/PTAA boundary. However, despite the observed reduction in halide segregation for the PTAA-coated MHP, more photoluminescence is emitted from iodide-rich domains in the presence of PTAA, which we attribute to preferential back-transfer of holes from PTAA to iodide-rich regions formed in close proximity to the interface. We further demonstrate that electronic traps generated near the interface between PTAA and the MHP, although present in high density, are ineffective drivers of halide segregation, while those that are prominent in the bulk are responsible for most of the halide segregation observed. Removal of such trap states at the MHP/PTAA interface with a piperidinium additive thus interestingly leads to more halide segregation occurring because, instead of channelling into interfacial states, charge carriers now accumulate in bulk trap states which are highly effective drivers of the segregation process. Overall, our work shows that interfacial trap states prominent at the MHP/PTAA interface do not contribute significantly to halide segregation throughout the bulk MHP and are efficiently passivated by a piperidinium salt. However, the presence of a PTAA layer leads to hole back-transfer from PTAA into iodide-rich regions near the interface that exhibit reduced interfacial energy offsets, adversely affecting photovoltaic performance. Such re-transferred holes may in turn exacerbate radiative recombination losses in the MHP beyond the detailed balance limit, by generating locally

strongly enhanced electron and hole densities. Careful passivation of trap states at the interface between MHP and charge-extraction layers therefore remains imperative for achieving high efficiencies in wide-bandgap photovoltaics devices.

4. Experimental Section

Sample Fabrication: $\text{FA}_{0.83}\text{Cs}_{0.17}\text{Pb}(\text{Br}_{0.4}\text{I}_{0.6})_3$ metal-halide perovskite (MHP) thin film samples were fabricated in line with a previous report^[64] with slight modification to account for the different substrate area. In summary, the precursors salts (formamidinium iodide, FAI, GreatCell Solar; cesium iodide, CsI, 99.99%, Alfa-Aesar; lead iodide, PbI_2 , 99.9%, TCI; lead bromide, PbBr_2 , >98%, Alfa-Aesar) were weighed stoichiometrically in an N_2 filled glovebox. The precursor salts were dissolved in a 4:1 ratio by volume of *N,N*-dimethylformamide (DMF, Sigma–Aldrich) to dimethyl sulfoxide (DMSO, Sigma–Aldrich), to a concentration of 1.3 M. The solution was stirred overnight before deposition. The ionic additive 1-butyl-1-methylpiperidinium tetrafluoroborate ($[\text{BMP}]^+[\text{BF}_4]^-$, purity 99%), purchased from Sigma–Aldrich, was dissolved in a 4:1 volume ratio of dimethylformamide (DMF) and dimethylsulfoxide (DMSO) and shaken overnight at room temperature. To mix the ionic additive into the precursor solution, an appropriate volume of the ionic additive solution was added to the perovskite precursor solution to obtain a perovskite concentration of 1.3 M for the precursor and 0.5 mg mL^{-1} of the ionic additive. Substrates made of z-cut quartz (area 1.3 cm^2) were cleaned by subsequent sonication in Decon90 (1 vol.% in deionised water), deionised water, acetone (Sigma–Aldrich) and isopropanol (Sigma–Aldrich) for 10 min each. The substrates were then dried using an N_2 gun before being treated with a UV-O_3 plasma for 12 min. The substrates were then immediately transferred into an N_2 filled glovebox prior to deposition of the perovskite layer. The perovskite films were fabricated using the following spincoating recipe: 50 μL of precursor solution was deposited dynamically onto the quartz substrate spinning at 1000 rpm. After 5 s, the substrate accelerated at 800 rpm s^{-1} , until it reached a final spin speed of 5000 rpm where it remained for 30 s. An antisolvent quench using 50 μL of Anisole (Sigma–Aldrich) was performed 5 s before the end of this step. The films were then annealed at 100°C for 30 min. PMMA (poly(methyl methacrylate), Sigma–Aldrich, mean molar weight 97000 g M^{-1}) was dissolved in chlorobenzene (Sigma–Aldrich) at 100 mg mL^{-1} . PTAA (poly(triaryl)amine) was purchased from Xi'an Polymer Light Technology Corp at a concentration of 75 mg mL^{-1} . To form the PMMA or PTAA films, 50 μL of solution was deposited statically onto the perovskite film. After 5 s, the substrate rotation was accelerated to 2000 rpm, for 25 s. The films were then annealed at 100°C for 5 min to drive off any residual solvent.

Absorbance Spectra: Absorbance spectra were acquired with the Fourier-transform infra-red (FTIR) technique using a Bruker Vertex 80v in transmission and reflection geometry. A silicon detector and CaF_2 beam-splitter were used, and a tungsten lamp as the light source. A silver mirror was used as the reflection reference, and vacuum as the transmission reference. Absorbance was calculated using $A = -\ln T/(1 - R)$.

In Situ XRD/PL Measurements: A custom-built insert was employed, as reported previously by Knight et al.,^[54] to measure concurrent, in situ X-ray diffraction (XRD) patterns and photoluminescence (PL) spectra. The setup consisted of an optical insert to a Rigaku SmartLab X-ray diffractometer, which supported illumination and PL collection optics. The illumination was provided by a fiber-coupled 470 nm diode laser (PicoQuant LDH-D-C-470, 190 mW cm^{-2} intensity), which was attached to the illumination optics of the insert using an optical fiber. The laser illumination was then launched into free space, directed at the sample. A lens was employed to control the illumination area, which was ensure to be larger than and overlap with the X-ray beam from the X-ray diffractometer. The collected PL was coupled into a fiber to lead it out of the Rigaku SmartLab, and analysed using an Ocean Optics USB2000 spectrometer. The XRD measurements were taken with a HyPix-3000 2D X-ray detector in a Bragg-Brentano reflection geometry, while the aforementioned optical insert was mounted into the Rigaku SmartLab

diffractometer. The incident radiation used was the Cu-K_{α1} line. The 2D detection sensor of the X-ray detector was used to capture a range of 2θ continuously without having to move any of the components, including the X-ray source, sample, or detector.

Time-resolved Photoluminescence Measurements: Time-resolved photoluminescence (TRPL) was measured in order to temporally investigate the charge-carrier dynamics using the time-correlated single photon counting (TCSPC) method. The same 470 nm diode laser used for in situ XRD/PL was employed (PicoQuant LDH-D-C-470), but set to pulsed mode with 1 MHz repetition rate. The PL emission was collected and coupled into a grating spectrometer (Princeton Instruments SP-2558). The PL emission was then directed to a photon-counting detector (PDM series from MPD). The timing was electronically controlled with a PicoHarp300 event timer. The measurements were conducted in ambient air, for compatibility with XRD/PL measurements. The TRPL data collated before halide segregation had occurred (Figure 3) was performed at three different sample spots and averaged, to remove any random spot-to-spot variations

Supporting Information

Supporting Information is available from the Wiley Online Library or from the author.

Acknowledgements

The authors gratefully acknowledge support from the Engineering and Physical Sciences Research Council (EPSRC), Prosperity Partnership (EP/S004947/1) and grant numbers EP/P033229/1 and EP/V010840/1. V.J.Y.L thanks Oxford Photovoltaics for doctoral support, and the Rank Prize for a Return to Research grant. A.J.K. thanks University College Oxford for graduate scholarship support from the Oxford-Radcliffe endowment. R.D.J.O. expresses his gratitude to the Penrose Scholarship for funding his studentship. L.M.H. thanks TUM-IAS for a Hans Fischer Senior Fellowship and Award.

Conflict of Interest

H.J.S. is founder and CSO of Oxford Photovoltaics Ltd, a company commercializing perovskite PV technology.

Data Availability Statement

The data that support the findings of this study are available from the corresponding author upon reasonable request.

Keywords

halide segregation, hole-transport layers, metal halide perovskites, passivation, perovskite solar cells, trap states

Received: April 28, 2022

Revised: July 7, 2022

Published online:

[1] S. Sahare, H. D. Pham, D. Angmo, P. Ghoderao, J. MacLeod, S. B. Khan, S. Lee, S. P. Singh, P. Sonar, *Adv. Energy Mater.* **2021**, *11*, 2101085.

- [2] M. Jeong, I. W. Choi, E. M. Go, Y. Cho, M. Kim, B. Lee, S. Jeong, Y. Jo, H. W. Choi, J. Lee, J.-H. Bae, S. K. Kwak, D. S. Kim, C. Yang, *Science* **2020**, *369*, 1615.
- [3] M. B. Johnston, L. M. Herz, *Acc. Chem. Res.* **2016**, *49*, 146.
- [4] H. J. Snaith, *Nat. Mater.* **2018**, *17*, 372.
- [5] A. K. Jena, A. Kulkarni, T. Miyasaka, *Chem. Rev.* **2019**, *119*, 3036.
- [6] S. De Wolf, J. Holovsky, S.-J. Moon, P. Löper, B. Niesen, M. Ledinsky, F.-J. Haug, J.-H. Yum, C. Ballif, *J. Phys. Chem. Lett.* **2014**, *5*, 1035.
- [7] S. D. Stranks, G. E. Eperon, G. Grancini, C. Menelaou, M. J. P. Alcocer, T. Leijtens, L. M. Herz, A. Petrozza, H. J. Snaith, *Science* **2013**, *342*, 341.
- [8] G. Xing, N. Mathews, S. Sun, S. S. Lim, Y. M. Lam, M. Gratzel, S. Mhaisalkar, T. C. Sum, *Science* **2013**, *342*, 344.
- [9] J. M. Ball, A. Petrozza, *Nat. Energy* **2016**, *1*, 16149.
- [10] T. Leijtens, G. E. Eperon, A. J. Barker, G. Grancini, W. Zhang, J. M. Ball, A. R. S. Kandada, H. J. Snaith, A. Petrozza, *Energy Environ. Sci.* **2016**, *9*, 3472.
- [11] W. Rehman, R. L. Milot, G. E. Eperon, C. Wehrenfennig, J. L. Boland, H. J. Snaith, M. B. Johnston, L. M. Herz, *Adv. Mater.* **2015**, *27*, 7938.
- [12] W. Rehman, D. P. McMeekin, J. B. Patel, R. L. Milot, M. B. Johnston, H. J. Snaith, L. M. Herz, *Energy Environ. Sci.* **2017**, *10*, 361.
- [13] A. Rajagopal, R. J. Stoddard, H. W. Hillhouse, A. K.-Y. Jen, *J. Mater. Chem. A* **2019**, *7*, 16285.
- [14] K. J. Savill, A. M. Ulatowski, L. M. Herz, *ACS Energy Lett.* **2021**, *6*, 2413.
- [15] T. C.-J. Yang, P. Fiala, Q. Jeangros, C. Ballif, *Joule* **2018**, *2*, 1421.
- [16] E. T. Hoke, D. J. Slotcavage, E. R. Dohner, A. R. Bowring, H. I. Karunadasa, M. D. McGehee, *Chem. Sci.* **2015**, *6*, 613.
- [17] R. E. Beal, D. J. Slotcavage, T. Leijtens, A. R. Bowring, R. A. Belisle, W. H. Nguyen, G. F. Burkhard, E. T. Hoke, M. D. McGehee, *J. Phys. Chem. Lett.* **2016**, *7*, 746.
- [18] W.-J. Yin, J.-H. Yang, J. Kang, Y. Yan, S.-H. Wei, *J. Mater. Chem. A* **2015**, *3*, 8926.
- [19] L. Protesescu, S. Yakunin, M. I. Bodnarchuk, F. Krieg, R. Caputo, C. H. Hendon, R. X. Yang, A. Walsh, M. V. Kovalenko, *Nano Lett.* **2015**, *15*, 3692.
- [20] G. E. Eperon, T. Leijtens, K. A. Bush, R. Prasanna, T. Green, J. T.-W. Wang, D. P. McMeekin, G. Volonakis, R. L. Milot, R. May, A. Palmstrom, D. J. Slotcavage, R. A. Belisle, J. B. Patel, E. S. Parrott, R. J. Sutton, W. Ma, F. Moghadam, B. Conings, A. Babayigit, H.-G. Boyen, S. Bent, F. Giustino, L. M. Herz, M. B. Johnston, M. D. McGehee, H. J. Snaith, *Science* **2016**, *354*, 861.
- [21] K. A. Bush, A. F. Palmstrom, Z. J. Yu, M. Boccard, R. Cheacharoen, J. P. Mailoa, D. P. McMeekin, R. L. Z. Hoye, C. D. Bailie, T. Leijtens, I. M. Peters, M. C. Minichetti, N. Rolston, R. Prasanna, S. Sofia, D. Harwood, W. Ma, F. Moghadam, H. J. Snaith, T. Buonassisi, Z. C. Holman, S. F. Bent, M. D. McGehee, *Nat. Energy* **2017**, *2*, 17009.
- [22] K. Xiao, R. Lin, Q. Han, Y. Hou, Z. Qin, H. T. Nguyen, J. Wen, M. Wei, V. Yeddu, M. I. Saidaminov, Y. Gao, X. Luo, Y. Wang, H. Gao, C. Zhang, J. Xu, J. Zhu, E. H. Sargent, H. Tan, *Nat. Energy* **2020**, *5*, 870.
- [23] A. Rajagopal, Z. Yang, S. B. Jo, I. L. Braly, P.-W. Liang, H. W. Hillhouse, A. K.-Y. Jen, *Adv. Mater.* **2017**, *29*, 1702140.
- [24] A. J. Knight, L. M. Herz, *Energy Environ. Sci.* **2020**, *13*, 2024.
- [25] A. J. Barker, A. Sadhanala, F. Deschler, M. Gandini, S. P. Senanayak, P. M. Pearce, E. Mosconi, A. J. Pearson, Y. Wu, A. R. Srimath Kandada, T. Leijtens, F. De Angelis, S. E. Dutton, A. Petrozza, R. H. Friend, *ACS Energy Lett.* **2017**, *2*, 1416.
- [26] S. Draguta, O. Shariya, S. J. Yoon, M. C. Brennan, Y. V. Morozov, J. S. Manser, P. V. Kamat, W. F. Schneider, M. Kuno, *Nat. Commun.* **2017**, *8*, 200.
- [27] G. Li, F. W. R. Rivarola, N. J. L. K. Davis, S. Bai, T. C. Jellicoe, F. de la Peña, S. Hou, C. Ducati, F. Gao, R. H. Friend, N. C. Greenham, Z.-K. Tan, *Adv. Mater.* **2016**, *28*, 3528.

- [28] P. Vashishtha, J. E. Halpert, *Chem. Mater.* **2017**, *29*, 5965.
- [29] I. L. Braly, R. J. Stoddard, A. Rajagopal, A. R. Uhl, J. K. Katahara, A. K.-Y. Jen, H. W. Hillhouse, *ACS Energy Lett.* **2017**, *2*, 1841.
- [30] P. S. Mathew, G. F. Samu, C. Janáky, P. V. Kamat, *ACS Energy Lett.* **2020**, *5*, 1872.
- [31] T. Elmelund, R. A. Scheidt, B. Seger, P. V. Kamat, *ACS Energy Lett.* **2019**, *4*, 1961.
- [32] Y. Shao, Y. Fang, T. Li, Q. Wang, Q. Dong, Y. Deng, Y. Yuan, H. Wei, M. Wang, A. Gruverman, J. Shield, J. Huang, *Energy Environ. Sci.* **2016**, *9*, 1752.
- [33] B. Yang, C. C. Brown, J. Huang, L. Collins, X. Sang, R. R. Unocic, S. Jesse, S. V. Kalinin, A. Belianinov, J. Jakowski, D. B. Geohegan, B. G. Sumpter, K. Xiao, O. S. Ovchinnikova, *Adv. Funct. Mater.* **2017**, *27*, 1700749.
- [34] J. S. Yun, J. Seidel, J. Kim, A. M. Soufiani, S. Huang, J. Lau, N. J. Jeon, S. I. Seok, M. A. Green, A. Ho-Baillie, *Adv. Energy Mater.* **2016**, *6*, 1600330.
- [35] F. Brivio, C. Caetano, A. Walsh, *J. Phys. Chem. Lett.* **2016**, *7*, 1083.
- [36] J. H. Noh, S. H. Im, J. H. Heo, T. N. Mandal, S. I. Seok, *Nano Lett.* **2013**, *13*, 1764.
- [37] D. P. McMeekin, G. Sadoughi, W. Rehman, G. E. Eperon, M. Saliba, M. T. Hörlantner, A. Haghighirad, N. Sakai, L. Korte, B. Rech, M. B. Johnston, L. M. Herz, H. J. Snaith, *Science* **2016**, *351*, 151.
- [38] G. F. Samu, C. Janáky, P. V. Kamat, *ACS Energy Lett.* **2017**, *2*, 1860.
- [39] T. Duong, H. K. Mulmudi, Y. Wu, X. Fu, H. Shen, J. Peng, N. Wu, H. T. Nguyen, D. Macdonald, M. Lockrey, T. P. White, K. Weber, K. Catchpole, *ACS Appl. Mater. Interfaces* **2017**, *9*, 26859.
- [40] S. Mahesh, J. M. Ball, R. D. J. Oliver, D. P. McMeekin, P. K. Nayak, M. B. Johnston, H. J. Snaith, *Energy Environ. Sci.* **2020**, *13*, 258.
- [41] S. G. Motti, J. B. Patel, R. D. Oliver, H. J. Snaith, M. B. Johnston, L. M. Herz, *Nat. Commun.* **2021**, *12*, 1.
- [42] A. J. Knight, J. B. Patel, H. J. Snaith, M. B. Johnston, L. M. Herz, *Adv. Energy Mater.* **2020**, *10*, 1903488.
- [43] E. J. Juarez-Perez, M. Wußler, F. Fabregat-Santiago, K. Lakus-Wollny, E. Mankel, T. Mayer, W. Jaegermann, I. Mora-Sero, *J. Phys. Chem. Lett.* **2014**, *5*, 680.
- [44] V. M. Le Corre, M. Stolterfoht, L. Perdigón Toro, M. Feuerstein, C. Wolff, L. Gil-Escrig, H. J. Bolink, D. Neher, L. J. A. Koster, *ACS Appl. Energy Mater.* **2019**, *2*, 6280.
- [45] J. M. Azpiroz, E. Mosconi, J. Bisquert, F. D. Angelis, *Energy Environ. Sci.* **2015**, *8*, 2118.
- [46] C. M. Wolff, P. Caprioglio, M. Stolterfoht, D. Neher, *Adv. Mater.* **2019**, *31*, 1902762.
- [47] S. Gharibzadeh, P. Fassel, I. M. Hossain, P. Rohrbeck, M. Frericks, M. Schmidt, M. R. Khan, T. Abzieher, B. A. Nejjand, F. Schackmar, et al., *Energy Environ. Sci.* **2021**, *14*, 5875.
- [48] A. J. Knight, A. D. Wright, J. B. Patel, D. P. McMeekin, H. J. Snaith, M. B. Johnston, L. M. Herz, *ACS Energy Lett.* **2019**, *4*, 75.
- [49] Z. Wang, Y. Wang, Z. Nie, Y. Ren, H. Zeng, *Nanoscale Adv.* **2019**, *1*, 4459.
- [50] M. Abdi-Jalebi, Z. Andaji-Garmaroudi, S. Cacovich, C. Stavrakas, B. Philippe, J. M. Richter, M. Alsari, E. P. Booker, E. M. Hutter, A. J. Pearson, S. Lilliu, T. J. Savenije, H. Rensmo, G. Divitini, C. Ducati, R. H. Friend, S. D. Stranks, *Nature* **2018**, *555*, 497.
- [51] J. T. DuBose, P. V. Kamat, *J. Am. Chem. Soc.* **2020**, *142*, 5362.
- [52] R. A. Belisle, K. A. Bush, L. Bertoluzzi, A. Gold-Parker, M. F. Toney, M. D. McGehee, *ACS Energy Lett.* **2018**, *3*, 2694.
- [53] R. A. Kerner, Z. Xu, B. W. Larson, B. P. Rand, *Joule* **2021**, *5*, 2273.
- [54] A. J. Knight, J. Borchert, R. D. J. Oliver, J. B. Patel, P. G. Radaelli, H. J. Snaith, M. B. Johnston, L. M. Herz, *ACS Energy Lett.* **2021**, *6*, 799.
- [55] T. Leijtens, K. A. Bush, R. Prasanna, M. D. McGehee, *Nat. Energy* **2018**, *3*, 828.
- [56] S. Tao, I. Schmidt, G. Brocks, J. Jiang, I. Tranca, K. Meerholz, S. Olthof, *Nat. Commun.* **2019**, *10*, 2560.
- [57] J. Endres, M. Kulbak, L. Zhao, B. P. Rand, D. Cahen, G. Hodes, A. Kahn, *J. Appl. Phys.* **2017**, *121*, 035304.
- [58] B. Conings, J. Drijkoningen, N. Gauquelin, A. Babayigit, J. D'Haen, L. D'Olielaeager, A. Ethirajan, J. Verbeeck, J. Manca, E. Mosconi, F. D. Angelis, H.-G. Boyen, *Adv. Energy Mater.* **2015**, *5*, 1500477.
- [59] F. Ünlü, E. Jung, J. Haddad, A. Kulkarni, S. Öz, H. Choi, T. Fischer, S. Chakraborty, T. Kirchartz, S. Mathur, *APL Mater.* **2020**, *8*, 070901.
- [60] Y. Tian, M. Peter, E. Unger, M. Abdellah, K. Zheng, T. Pullerits, A. Yartsev, V. Sundström, I. G. Scheyblykin, *Phys. Chem. Chem. Phys.* **2015**, *17*, 24978.
- [61] J. F. Galisteo-López, M. Anaya, M. E. Calvo, H. Míguez, *J. Phys. Chem. Lett.* **2015**, *6*, 2200.
- [62] J. S. Godding, A. J. Ramadan, Y.-H. Lin, K. Schutt, H. J. Snaith, B. Wenger, *Joule* **2019**, *3*, 2716.
- [63] R. Brenes, C. Eames, V. Bulović, M. S. Islam, S. D. Stranks, *Adv. Mater.* **2018**, *30*, 1706208.
- [64] Y.-H. Lin, N. Sakai, P. Da, J. Wu, H. C. Sansom, A. J. Ramadan, S. Mahesh, J. Liu, R. D. J. Oliver, J. Lim, L. Aspirtarte, K. Sharma, P. K. Madhu, A. B. Morales-Vilches, P. K. Nayak, S. Bai, F. Gao, C. R. M. Grovenor, M. B. Johnston, J. G. Labram, J. R. Durrant, J. M. Ball, B. Wenger, B. Stannowski, H. J. Snaith, *Science* **2020**, *369*, 96.
- [65] R. D. J. Oliver, P. Caprioglio, F. Peña-Camargo, L. R. V. Buizza, F. Zu, A. J. Ramadan, S. G. Motti, S. Mahesh, M. M. McCarthy, J. H. Warby, Y.-H. Lin, N. Koch, S. Albrecht, L. M. Herz, M. B. Johnston, D. Neher, M. Stolterfoht, H. J. Snaith, *Energy Environ. Sci.* **2022**, *15*, 714.
- [66] M. C. Brennan, S. Draguta, P. V. Kamat, M. Kuno, *ACS Energy Lett.* **2018**, *3*, 204.
- [67] P. Nandi, C. Giri, D. Swain, U. Manju, S. D. Mahanti, D. Topwal, *ACS Appl. Energy Mater.* **2018**, *1*, 3807.
- [68] W. Mao, C. R. Hall, S. Bernardi, Y.-B. Cheng, A. Widmer-Cooper, T. A. Smith, U. Bach, *Nat. Mater.* **2021**, *20*, 55.
- [69] L. Krückemeier, B. Krogmeier, Z. Liu, U. Rau, T. Kirchartz, *Adv. Energy Mater.* **2021**, *11*, 2003489.
- [70] T. J. Jacobsson, J.-P. Correa-Baena, M. Pazoki, M. Saliba, K. Schenk, M. Grätzel, A. Hagfeldt, *Energy Environ. Sci.* **2016**, *9*, 1706.
- [71] P. Caprioglio, S. Caicedo-Dávila, T. C.-J. Yang, C. M. Wolff, F. Peña-Camargo, P. Fiala, B. Rech, C. Ballif, D. Abou-Ras, M. Stolterfoht, S. Albrecht, Q. Jeangros, D. Neher, *ACS Energy Lett.* **2021**, *6*, 419.
- [72] M. Stolterfoht, P. Caprioglio, C. M. Wolff, J. A. Márquez, J. Nordmann, S. Zhang, D. Rothhardt, U. Hörmann, Y. Amir, A. Redinger, L. Kegelmann, F. Zu, S. Albrecht, N. Koch, T. Kirchartz, M. Saliba, T. Unold, D. Neher, *Energy Environ. Sci.* **2019**, *12*, 2778.
- [73] T. C. Sum, M. Righetto, S. S. Lim, *J. Chem. Phys.* **2020**, *152*, 130901.
- [74] L. M. Herz, *Ann. Phys. Chem.* **2016**, *67*, 65.
- [75] R. G. Balakrishna, S. M. Kobosko, P. V. Kamat, *ACS Energy Lett.* **2018**, *3*, 2267.
- [76] W. Li, M. U. Rothmann, A. Liu, Z. Wang, Y. Zhang, A. R. Pascoe, J. Lu, L. Jiang, Y. Chen, F. Huang, Y. Peng, Q. Bao, J. Etheridge, U. Bach, Y.-B. Cheng, *Adv. Energy Mater.* **2017**, *7*, 1700946.
- [77] X. Tang, M. van den Berg, E. Gu, A. Horneber, G. J. Matt, A. Osvet, A. J. Meixner, D. Zhang, C. J. Brabec, *Nano Lett.* **2018**, *18*, 2172.
- [78] C. Ran, J. Xu, W. Gao, C. Huang, S. Dou, *Chem. Soc. Rev.* **2018**, *47*, 4581.
- [79] H. Jin, E. Debroye, M. Keshavarz, I. G. Scheyblykin, M. B. J. Roeffaers, J. Hofkens, J. A. Steele, *Mater. Horiz.* **2020**, *7*, 397.
- [80] D. Meggiolaro, F. De Angelis, *ACS Energy Lett.* **2018**, *3*, 2206.

- [81] D. Meggiolaro, S. G. Motti, E. Mosconi, A. J. Barker, J. Ball, C. Andrea Riccardo Perini, F. Deschler, A. Petrozza, F. De Angelis, *Energy Environ. Sci.* **2018**, *11*, 702.
- [82] G. Kim, A. Petrozza, *Adv. Energy Mater.* **2020**, *10*, 2001959.
- [83] J.-N. Yang, Y. Song, J.-S. Yao, K.-H. Wang, J.-J. Wang, B.-S. Zhu, M.-M. Yao, S. U. Rahman, Y.-F. Lan, F.-J. Fan, H.-B. Yao, *J. Am. Chem. Soc.* **2020**, *142*, 2956.
- [84] A. Ruth, M. C. Brennan, S. Draguta, Y. V. Morozov, M. Zhukovsky, B. Janko, P. Zapol, M. Kuno, *ACS Energy Lett.* **2018**, *3*, 2321.
- [85] S. J. Yoon, M. Kuno, P. V. Kamat, *ACS Energy Lett.* **2017**, *2*, 1507.
- [86] M. C. Brennan, A. Ruth, P. V. Kamat, M. Kuno, *Trends Chem.* **2020**, *2*, 282.